NANO · MICRO small
www.small-journal.com

Platelet Membrane-Derived Nanodiscs for Neutralization of Endogenous Autoantibodies and Exogenous Virulence Factors

Lei Sun, Yiyan Yu, Yifei Peng, Dan Wang, Shuyan Wang, Ilkoo Noh, Ronnie H. Fang, Weiwei Gao, and Liangfang Zhang**

The multifaceted functions of platelets in various physiological processes have long inspired the development of therapeutic nanoparticles that mimic specific platelet features for disease treatment. Here, the development and characterization of platelet membrane-derived nanodiscs (PLT-NDs) as platelet decoys for biological neutralization is reported. In one application, PLT-NDs effectively bind with anti-platelet autoantibodies, thus blocking them from interacting with platelets. In a mouse model of thrombocytopenia, PLT-NDs successfully neutralize pathological anti-platelet antibodies, preventing platelet depletion and maintaining hemostasis. In another application, PLT-NDs effectively neutralize the cytotoxicity of bacterial virulence factors secreted by methicillin-resistant *Staphylococcus aureus* (MRSA). In a mouse model of MRSA infection, treatment with PLT-NDs leads to significant survival benefits for the infected mice. Additionally, PLT-NDs show good biocompatibility and biosafety, as demonstrated in acute toxicity studies conducted in mice. These findings underscore the potential of PLT-NDs as a promising platelet mimicry for neutralizing various biological agents that target platelets. Overall, this work expands the repertoire of platelet-mimicking nanomedicine by creating a unique disc-like nanostructure made of natural platelet membranes.

1. Introduction

Platelets are specialized blood cells involved in numerous physiological processes, including responding to vascular damage response, recognizing tumor cells, and interacting with pathogens.[1–3] The versatile functions and dynamic biointerfacing abilities exhibited by platelets have inspired the development of platelet-mimicking nanoparticle platforms aimed at replicating platelet properties to enhance their effectiveness in disease treatment.[4–6] One approach to achieving biomimicry is to replicate the physical characteristics of platelets, such as their geometry and mechanical properties. Nanoparticles designed to mimic the discoidal geometry of resting platelets or the spiny shape of the activated platelets offer a larger contact surface area than their spherical counterpart.[7,8] Another strategy involves mimicking platelet surface biological functions by coating nanoparticle substrates with platelet membranes.[9–13] This process faithfully transfers various membrane proteins from platelets onto synthetic nanoparticles, which are difficult to achieve through traditional chemical methods. Consequently, these nanoparticles exhibit exceptional biointerfacing properties, including improved stealth, selective adhesion to damaged blood vessels, and the ability to target cancer or platelet-adhering pathogens. Furthermore, another approach is to incorporate platelet-simulating molecules into nanoparticles to mimic their pro-coagulant functions. For instance, nanoparticles conjugated with phosphatidylserine promote thrombin amplification and fibrin generation, while those linked with synthetic peptides display enhanced binding with exposed collagen at the wound site through helicogenic interactions.[7,14–16]

As platelet-mimicking nanoparticles gain increasing attention in recent nanotechnological advancements, a new biomimetic nanoparticle platform has emerged, involving the use of cell membranes to synthesize nanodiscs (NDs) for therapeutic applications.[17,18] These cell membrane-derived NDs (referred to as "cellular NDs" or "CNDs") are small pieces of natural cell membranes surrounded by scaffolding stabilizers. Similar to NDs made from synthetic lipids, they are typically less than 20 nm in diameter.[19,20] The compact size and the discoidal shape enhance the mobility of CNDs, enabling them to navigate tight junctions and penetrate deep tissues effectively.[21,22] What distinguishes CNDs from synthetic NDs is their cell-mimicking functions inherited from the source cell membranes. For instance, CNDs made from bacterial outer membranes have been developed for antibacterial vaccination.[17] These CNDs efficiently

L. Sun, Y. Yu, Y. Peng, D. Wang, S. Wang, I. Noh, R. H. Fang, W. Gao, L. Zhang
Department of NanoEngineering
Chemical Engineering Program
Shu and K.C. Chien and Peter Farrell Collaboratory
University of California San Diego
La Jolla, CA 92093, USA
E-mail: w5gao@ucsd.edu; zhang@ucsd.edu

The ORCID identification number(s) for the author(s) of this article can be found under https://doi.org/10.1002/smll.202308327

DOI: 10.1002/smll.202308327

traverse the lymphatic system, reaching and interacting with antigen-presenting cells in the lymph nodes. Unlike synthetic ND vaccines, these bacterial membrane-derived CNDs present natural immunogenic antigens with intrinsic adjuvant properties and pathogen-associated molecular patterns that stimulate innate and adaptive immune responses. This unique combination of features makes them highly effective in activating the immune system. Moreover, CNDs made from red blood cell (RBC) membrane have also been designed for bacterial toxin neutralization.[18] Besides being significantly smaller than RBC membrane vesicles and displaying improved stability in biological solutions, these CNDs mimic the characteristics of parent RBCs, allowing them to bind with a wide range of pore-forming toxins (PFTs).

In this study, we draw inspiration from the remarkable properties of platelets and the compelling attributes of CNDs to synthesize platelet membrane-derived NDs (referred to as "PLT-NDs") and explore their therapeutic potentials (**Figure 1A**). Our primary focus is to use PLT-NDs for biological neutralization to treat two disease models, including immune thrombocytopenic purpura (ITP) caused by endogenous pathological autoantibodies and infection caused by methicillin-resistant *Staphylococcus aureus* bacteria (MRSA). In ITP, the production of anti-platelet antibodies (PLT-Abs) reduces platelet counts, resulting in severe and uncontrollable bleeding that can be life-threatening.[23,24] PLT-NDs contain a comprehensive array of platelet surface proteins, implying that they can act as decoys to scavenge and neutralize these PLT-Abs. Consequently, treatment with PLT-NDs is expected to alleviate the burden of the disease. In the case of MRSA infection, bacterial pathogenesis is fueled by secreted virulence factors, including PFTs with diverse host targets.[25,26] Our hypothesis is that PLT-NDs can function as decoys to bind and neutralize *S. aureus* virulence factors, diverting them from their intended cellular targets. By doing so, PLT-NDs can preserve host cell defense functions, aiding in bacterial clearance.

2. Results and Discussion

We collected platelets from mouse whole blood and derived the membrane using a centrifugation method previously established.[9] We then sonicated the platelet membrane to form membrane vesicles (PLT-vesicles) and mixed them with styrene maleic acid copolymer-lipid particles 200 (SMA). As a result of this mixing, the size of the PLT vesicles reduced significantly, from an initial size of 149.6 ± 4.6 nm to a final size of 17.3 ± 1.4 nm. However, the zeta potential values before (−19.8 ± 1.0 mV) and after (−17.5 ± 0.7 mV) the mixing remained comparable (Figure 1B). Meanwhile, the transmission electron microscopy (TEM) study revealed disc-shaped nanostructures with uniform size distribution (Figure 1C). These results are consistent with previous CND formulation and characterization, indicating the successful formation of PLT-NDs.[17,18] When stored in 1× phosphate-buffered saline (PBS) at 4 °C for 7 days or 50% fetal bovine serum (FBS) at 37 °C for 72 h, PLT-ND samples showed negligible change in size, demonstrating good buffer storage stability and biostability (Figure 1D).

We investigated PLT-ND pharmacokinetic (PK) and biodistribution profiles in mice. To assess the PK profile, we labeled PLT-NDs with Alexa Fluor 647 and administered the dye-labeled NDs (AF647-PLT-NDs) via the tail vein at 30 mg kg^{-1} (protein concentration). We collected blood samples at various time points and measured the fluorescence intensity. Initially, there was a rapid decline in the PLT-ND signal after the injection, but this decay rate slowed significantly after ≈5 h. Using a two-compartment model applied in previous nanoparticle circulation studies, we calculated the elimination half-life of PLT-NDs to be 16.4 h, comparable to the half-life reported for other CNDs (Figure 1E).[17,18] In the biodistribution study, we also injected AF647-PLT-NDs into mice through the tail vein at 30 mg kg^{-1} (membrane protein) and measured fluorescence intensities from the heart, liver, spleen, lung, kidney, and blood (Figure 1F). When normalized per gram of tissue, we observed that the NDs were predominantly localized in the liver and spleen, the primary organs of the reticuloendothelial system (RES). Moreover, when analyzed per organ, the NDs were mainly distributed in the liver and spleen. Concurrently, substantial fluorescence was observed in the blood at different time points. As the blood fluorescence signal decreased, the signal in the liver increased, suggesting that the RES is responsible for PLT-ND clearance.

After formulating PLT-NDs, we investigated their specificity and capacity to bind with PLT-Abs. To quantify the antibody amount bound to PLT-NDs, we labeled the antibodies with fluorescein isothiocyanate (FITC-PLT-Abs). Additionally, we modified PLT-NDs with azido groups (N_3-PLT-ND). After mixing the two moieties, the binding reaction occurred. After the reaction, we added dibenzocyclooctyl (DBCO)-modified agarose beads to the reaction mixture. Agarose beads capture the NDs via click chemistry, allowing us to isolate and quantify antibodies bound to the PLT-NDs (**Figure 2A**). As shown in Figure 2B, PLT-NDs mixed with FITC-PLT-Abs exhibited a pronounced FITC fluorescence signal, indicating robust binding interactions. In contrast, the control NDs formulated with RBC membrane (RBC-NDs) mixed with the antibody displayed negligible FITC signal. This stark contrast in antibody binding highlighted the binding specificity arising from the intrinsic properties of the platelet membrane used in the PLT-ND formulation. Notably, the binding of PLT-NDs with PLT-Abs generated comparable FITC signals in 1× PBS and 50% mouse serum. This observation suggested that the binding was not affected by the presence of serum proteins, underscoring the potential of PLT-NDs to retain their functionality in complex in vivo environments. Using the same methodology, we assessed PLT-ND binding capacity against PLT-Abs. For this study, we kept FITC-PLT-Ab input fixed at 30 μg mL^{-1} and varied PLT-ND concentrations from 0 to 8 μg mL^{-1}. As depicted in Figure 2C, an increase in PLT-ND concentration led to a corresponding increase in the bound antibody. At ≈1 μg mL^{-1} of PLT-NDs, 50% of the antibody was bound (EC50, PLT-ND: PLT-Ab = 1:15, weight ratio). The bound antibody reached a plateau when the PLT-ND concentration exceeded 4 μg mL^{-1}, indicating that 4 μg mL^{-1} of PLT-NDs were sufficient to bind 100% of the antibody (EC100, PLT-ND: PLT-Ab = 1:7.5, weight ratio). In a different experiment, we fixed PLT-ND concentration (25 μg mL^{-1}) and incubated them with various concentrations of FITC-PLT-Abs. As shown in Figure 2D, plotting the bound PLT-Abs against the logarithm of PLT-Abs input yielded a typical sigmoid binding profile. From this measurement, the EC50 value of the PLT-ND binding with PLT-Abs was calculated to be 47 μg mL^{-1}.[27]

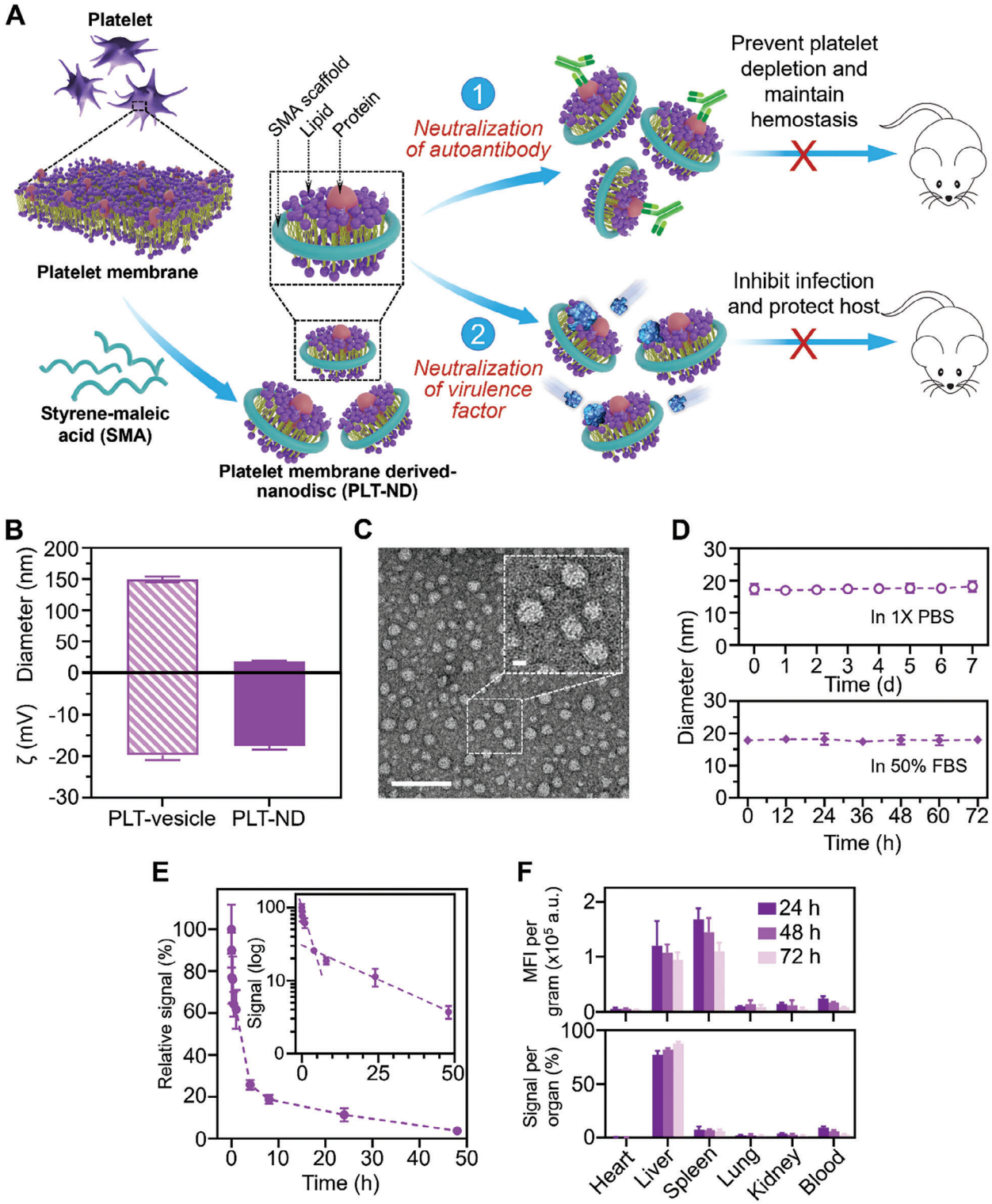

Figure 1. Preparation and characterization of platelet membrane-derived NDs (PLT-NDs). A) Schematic preparation of PLT-NDs and their mechanisms of action in treating immune thrombocytopenic purpura (ITP) and infection by methicillin-resistant *S. aureus* (MRSA). B) Size (diameter) and zeta potential (mV) measurement of platelet vesicles and PLT-NDs using dynamic light scattering (DLS). C) Representative transmission electron microscopy (TEM) image of PLT-NDs (scale bar: 100 nm). Insert: a zoom-in view of PLT-NDs (scale bar: 10 nm). D) Stability of PLT-NDs, measured as size with DLS, in 1× PBS at 4 °C for 7 days and 50% fetal bovine serum (FBS) at 37 °C for 72 h. E) Pharmacokinetic profile of PLT-NDs after intravenous injection of Alexa Fluor 647-labeled PLT-NDs (AF647-PLT-NDs). F) Biodistribution of PLT-NDs in mice at 24, 48, and 72 h after intravenous injection of AF647-PLT-NDs. In all datasets, $n = 3$ independent experiments using the same batch of mouse platelet membrane. In (E) and (F), PLT-ND dosage was 30 mg kg^{-1} (membrane protein). Data in (B) and (F) are presented as mean + s.d., while data in (D) and (E) are presented as mean ± s.d.

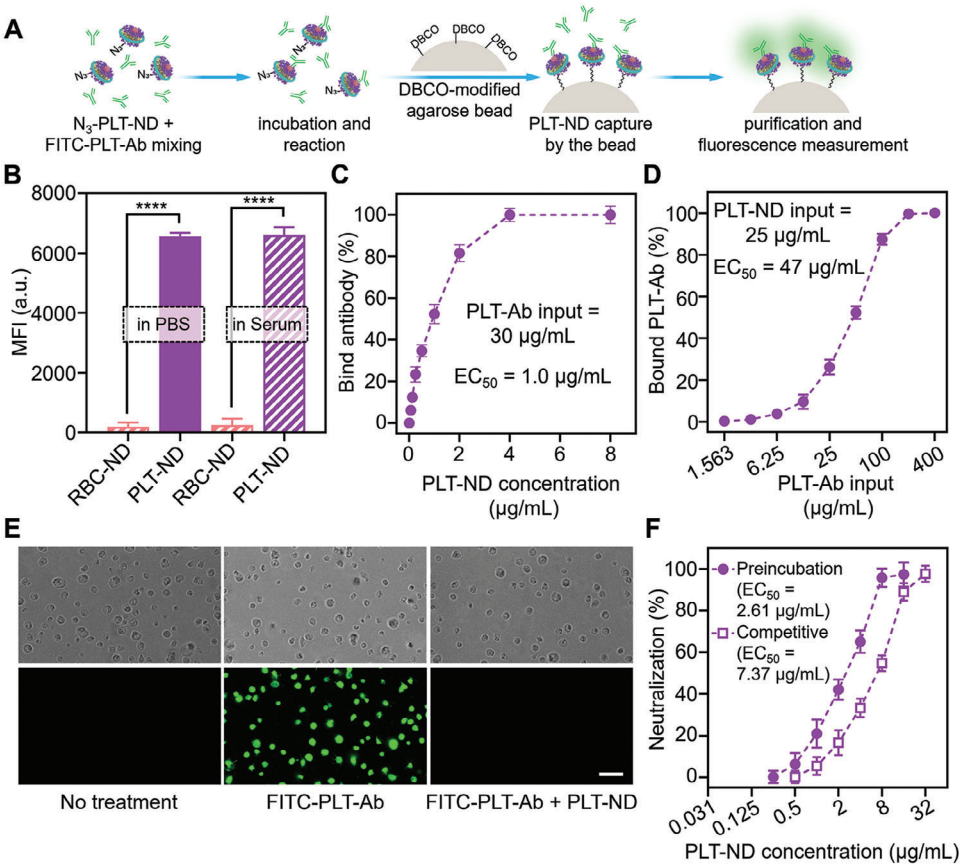

Figure 2. In vitro neutralization of anti-platelet antibodies (PLT-Abs) by PLT-NDs. A) Schematic separation of fluorescein isothiocyanate (FITC)-labeled PLT-Abs bound to azido functionalized PLT-NDs (N_3-PLT-NDs) or azido functionalized red blood cell (RBC)-derived NDs (N_3-RBC-NDs) by dibenzocyclooctyl (DBCO) functionalized agarose beads via click chemistry reaction. B) Binding of PLT-Abs to RBC-NDs or PLT-NDs in 1× PBS or 50% mouse serum (MFI: mean fluorescence intensity). C) Relative binding of PLT-Abs (30 μg/mL) to PLT-NDs at various concentrations. D) Relative binding of PLT-Abs at various concentrations to PLT-NDs (25 μg mL^{-1}). E) Fluorescence images of platelets treated with 1× PBS (no treatment group), FITC-PLT-Abs, or FITC-PLT-Abs bound PLT-NDs. Scale bar = 10 μm. F) The neutralization rate of PLT-Abs by PLT-NDs in preincubation and competitive regimens. In all studies, $n = 3$ independent experiments using the same batch of mouse platelet membrane. Data in (B) is presented as mean + s.d. Data in (C), (D), and (F) are presented as mean ± s.d., $^{****}p \leq 0.0001$. Statistical analysis was performed by using a Student's *t*-test (two-tailed).

We next examined the neutralization of PLT-NDs against PLT-Abs in vitro. For the qualitative analysis, we combined PLT-NDs (10 μg mL^{-1}) with FITC-PLT-Abs (20 μg mL^{-1}) and introduced the mixture to a platelet suspension. We examined the platelets for the bound antibodies using a laser scanning confocal microscope (LSCM). As shown in Figure 2E, the platelets treated with FITC-PLT-Abs exhibited a robust green fluorescence signal, indicating successful antibody binding. However, when the platelets were treated with the preincubated mixture of PLT-NDs and FITC-PLT-Abs, the FITC fluorescence diminished. This result shows that the binding between PLT-Ab and PLT-ND is strong enough to prevent PLT-Ab from attacking platelets. For the quantitative investigation, we measured antibody neutralization by PLT-NDs in two different regimens. In a preincubation regimen, we mixed various concentrations of PLT-NDs with FITC-PLT-Abs (20 μg mL^{-1}) and then added the mixtures to platelets. We quantified the platelet-bound antibody using flow cytometry. The EC50 value, representing the PLT-ND concentration that neutralized 50% of the antibodies, was found to be 2.61 μg mL^{-1}, while 8 μg mL^{-1} of PLT-NDs were required to neutralize all antibodies (EC100, Figure 2F). In a competitive regimen, we mixed various concentrations of PLT-NDs with platelets first and then added FITC-PLT-Abs (20 μg mL^{-1}) to the mixture. In this case, the EC50 and EC100 values were measured to be 7.37 μg mL^{-1} and 32 μg mL^{-1}, respectively. These findings demonstrated that PLT-NDs were highly effective in neutralizing PLT-Abs in vitro.

After confirming the in vitro neutralization of PLT-Abs, we proceeded to evaluate the in vivo efficacy using a mouse model of ITP.[28,29] Specifically, we intraperitoneally injected mice with PLT-Abs at a dosage of 50 μg per mouse to induce thrombocytopenia and administered various dosages of PLT-NDs 15 min after the antibody injection (**Figure 3A**). Following the antibody injection, the platelet counts continuously dropped and reached the lowest level of ≈10% of its original value at ≈24 h.[28,29] After 24 h of the PLT-ND injection, we sampled blood and measured platelet counts as an indication of effectiveness. As shown in Figure 3B, platelet counts in mice injected with PLT-Abs but without PLT-ND treatment dropped sharply to ≈10% of the baseline level. However, mice that were administered the antibody and also received PLT-ND treatment showed higher platelet counts,

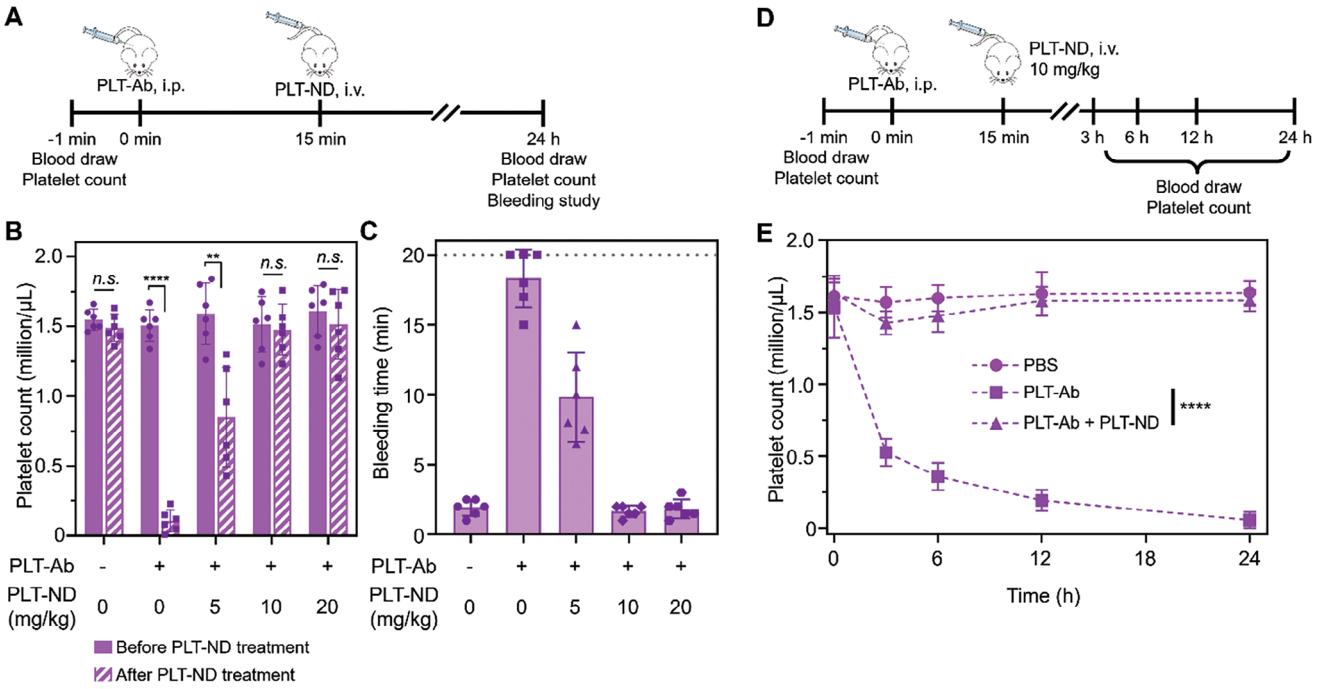

Figure 3. In vivo efficacy of PLT-NDs for the treatment of ITP. A) Study protocol of treating antibody-induced ITP with PLT-NDs in a mouse model. B) Platelet counts of mice before and 24 h after PLT-Abs injection. Mice were first injected intraperitoneally with PLT-Abs (50 μg per mouse), followed by intravenous administration of PLT-NDs at various dosages (5, 10, and 20 mg kg^{-1}) 15 min later. Healthy mice were intravenously injected with 1× PBS as the control group and their platelet counts serve as a baseline. C) Bleeding time of mice after 24 h after PLT-Abs injection. Mice with bleeding time over 20 min were euthanized. D) Study protocol of treating antibody-induced ITP with PLT-NDs in mice and collecting blood for analyzing platelet counts at different time points. E) Platelet counts of mice treated with PBS, PLT-Ab, and PLT-Ab followed by 10 mg kg^{-1} PLT-ND at different time points. In all studies, $n = 6$ mice. Data in (B–D) are presented as mean ± s.d. $^{**}p \leq 0.01$, $^{****}p \leq 0.0001$, *n.s.*: not significant. Statistical analysis was performed using one-way ANOVA with Tukey's post-hoc test.

indicating successful neutralization of PLT-Abs and platelet protection by PLT-NDs. Moreover, mice treated with 5, 10, and 20 mg kg^{-1} of PLT-NDs maintained 53.4%, 97.4%, and 95.1% of their baseline platelet values, respectively. We also conducted a bleeding time assay to assess the antibody neutralization effectiveness of PLT-NDs.[30] In this assay, we measured the time it took for bleeding to cease after excising the tail tips of mice. For mice without ITP, the bleeding typically stopped within 1–2.5 min after excision (Figure 3C). ITP mice that did not receive PLT-NDs exhibited a significantly prolonged bleeding time, lasting no less than 15 min. In contrast, mice treated with varying dosages of PLT-NDs showed a decrease in bleeding time corresponding to the increasing PLT-ND dosages. At a PLT-ND dosage of 10 and 20 mg kg^{-1}, the bleeding time was comparable to that observed in healthy control mice. The platelet counts and the bleeding time correlate, confirming the in vivo effectiveness of PLT-NDs in neutralizing PLT-Abs in a dose-dependent manner.

We also investigated the kinetics of PLT count recovery (Figure 3D). In this study, mice were intraperitoneally injected with PLT-Abs (50 μg per mouse). After 15 min, they received an intravenous injection of PLT-NDs at 10 mg kg^{-1} via the tail vein. Platelet counts were recorded at various time points. Mice injected intravenously with 1× PBS or PLT-Abs alone served as controls. As shown in Figure 3E, intraperitoneal administration of PLT-Abs induced significant thrombocytopenia, with a drastic reduction in platelet counts over time post-injection. Notably, mice injected with PLT-Abs and treated with PLT-NDs displayed platelet counts comparable to those injected with PBS, indicating effective neutralization of PLT-Abs by PLT-NDs and prevention of platelet depletion.

Besides endogenous autoantibodies, we also investigated the capability and capacity of PLT-NDs in neutralizing exogenous virulence factors secreted by bacteria. We selected α-toxin, a representative virulence factor, to assess the neutralization effect.[31] When platelets were incubated with α-toxin, we observed a substantial release of lactate dehydrogenase (LDH), indicating cytotoxicity induced by the α-toxin (**Figure** 4A). However, when α-toxin was incubated with PLT-NDs, in a preincubation regimen (α-toxin mixed with PLT-NDs followed by the addition to platelets) or a competitive regimen (PLT-NDs were added to platelets followed by the addition of α-toxin), the LDH levels were comparable to untreated platelets, suggesting that PLT-NDs effectively neutralized the α-toxin. Furthermore, we investigated the protective effect of PLT-NDs against MRSA bacterial whole-secreted proteins (wSP). Treatment with wSP led to a significant increase in platelet LDH levels, indicating cytotoxicity. In contrast, when wSP was treated with PLT-NDs in a preincubation regimen (wSP mixed with PLT-NDs followed by the addition to platelets) or a competitive regimen (PLT-NDs were added to platelets followed by the addition of wSP), the LDH levels were substantially lower, suggesting effective neutralization of

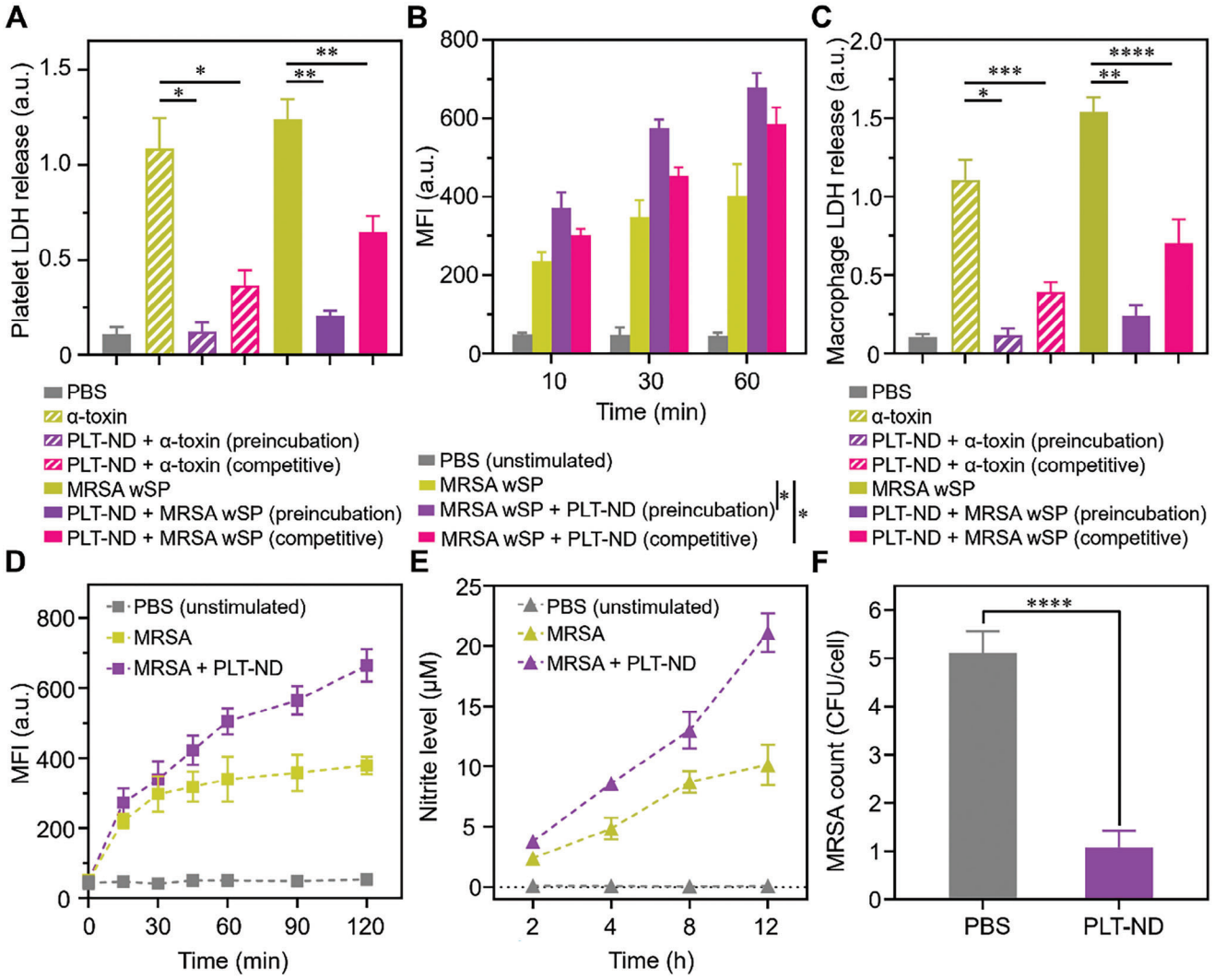

Figure 4. In vitro neutralization of MRSA infection by PLT-NDs. A) Quantification of lactate dehydrogenase (LDH) levels after treating platelets with PBS, α-toxin, PLT-ND plus α-toxin, MRSA wSP, or PLT-ND plus MRSA wSP. B) Quantification of P-selectin expression levels at various time points after treating platelets with PBS, MRSA wSP, or PLT-ND plus MRSA wSP. C) Quantification of LDH levels after treating J774 mouse macrophages with PBS, α-toxin, PLT-ND plus α-toxin, MRSA wSP, or PLT-ND plus MRSA wSP. D) Quantification of reactive oxygen species (ROS) levels at various time points when treating J774 cells with PBS, MRSA wSP, or PLT-ND plus MRSA wSP. E) Quantification of nitrite levels at various time points when treating J774 cells with PBS, MRSA wSP, or PLT-ND plus MRSA wSP. F) Intracellular MRSA bacteria in J774 cells after infection with MRSA added with PBS or PLT-NDs. Data in A–C, F) are presented as mean + s.d. Data in D–E) are presented as mean ± s.d. $^{*}p \leq 0.05$, $^{****}p \leq 0.0001$. Statistical analysis was performed with a Student's *t*-test (two-tailed).

multiple and complex virulence factors secreted by MRSA bacteria. We also measured the P-selectin expression on platelets in response to the neutralization of virulence factors by PLT-NDs, as a higher P-selectin expression correlates to a higher bactericidal activity.[32,33] Exposure of platelets to MRSA wSP in a preincubation or competitive regimen resulted in a significantly higher P-selectin expression in a time-dependent manner than platelets treated with MRSA wSP only, indicating that PLT-ND neutralization of the virulence factors improved this essential platelet response function (Figure 4B).

Next, we investigated the impact of neutralizing the virulence factors by PLT-NDs on macrophages. Figure 4C shows that macrophage exposure to α-toxin in a preincubation regimen or a competitive regimen resulted in a significantly higher level of LDH release than α-toxin treated with PLT-NDs. A similar response of LDH levels was observed when MRSA wSP, confirming the neutralization of MRSA virulence factors by PLT-NDs. We hypothesized that neutralization of the virulence factors would boost macrophage bactericidal activity. In the study, macrophages produced a higher level of reactive oxygen species (ROS) when mixed with MRSA treated with PLT-NDs than MRSA only (Figure 4D). Similarly, when macrophages were mixed with MRSA treated with PLT-NDs, they produced more nitric oxide than MRSA only (Figure 4E). Higher levels of ROS and nitric oxide are the hallmarks of macrophage defense against bacteria.[34–36] As shown in Figure 4F, we observed a lower intracellular infection of MRSA bacteria in macrophages after the bacteria were treated with PLT-NDs, confirming that neutralizing

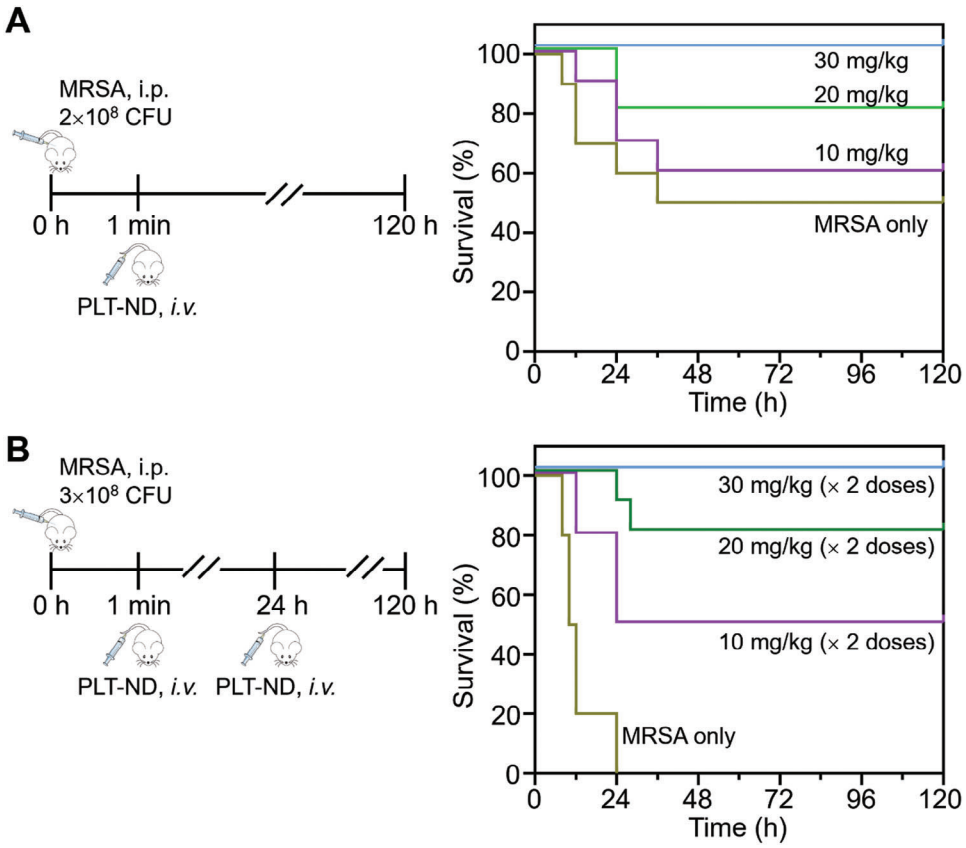

Figure 5. In vivo therapeutic efficacy of PLT-NDs against MRSA infection. A) In the first therapeutic study, mice were first challenged with 2×10^8 CFU MRSA bacteria per mouse. These mice received a single injection of PBS buffer or different dosages of PLT-NDs (10, 20, and 30 mg kg^{-1}) at 1 min after the injection of MRSA. The survival rates were monitored for 120 h. B) In the second therapeutic study, mice were first challenged with 3×10^8 CFU MRSA bacteria per mouse. These mice received two injections of PBS buffer or different dosages of PLT-NDs (10, 20, and 30 mg kg^{-1}) at 1 min and 24 h after the injection of MRSA. In all datasets, $n = 10$ mice. Statistical analysis was performed using Log-rank and Mantel-Cox test.

the virulence factors by PLT-NDs led to a more potent MRSA killing by macrophages.

After confirming the ability of PLT-NDs to neutralize MRSA virulence factors in vitro, we proceeded to evaluate their therapeutic efficacy in vivo using a mouse model of MRSA infection. By effectively absorbing and neutralizing various bacterial virulence factors, we expect PLT-NDs to preserve platelet activation and facilitate macrophage-mediated bactericidal activity, thereby enabling survival benefits in an MRSA infection model.[33] In the study, we injected mice with 2×10^8 colony formation unit (CFU) of MRSA intraperitoneally and then administered various dosages of PLT-NDs intravenously through the tail vein 1 min later (**Figure** 5A). Mouse survival was monitored for 120 h. MRSA administration alone resulted in a 50% mortality rate. When mice were treated with PLT-NDs at 10, 20, and 30 mg kg^{-1}, the survival rates increased to 60%, 80%, and 100%, respectively. The dose-dependent survival benefit clearly showed the effectiveness of PLT-NDs for treating MRSA infection. To further confirm the effectiveness, we administered a higher MRSA dose of 3×10^8 CFU to each mouse intraperitoneally and monitored mouse survival for 120 h (Figure 5B). This time, mice received two injections of PLT-NDs at 1 and 24 h after the MRSA injection. Mice that received MRSA alone exhibited 100% mortality. However, when mice were challenged with MRSA and also received injections of PLT-NDs at dosages of 10, 20, and 30 mg kg^{-1}, their survival rates increased to 50%, 80%, and 100%, respectively. These results provide strong evidence for the efficacy of PLT-NDs for the treatment of MRSA infection in vivo.

Finally, we evaluated the acute toxicity of PLT-ND in vivo in healthy mice. PLT-NDs were injected intravenously through the tail vein at 30 mg kg^{-1}, the highest concentration used in this study. After 24 h of PLT-ND administration, we examined the RBC, platelet, and white blood cell counts, and their values were found to be comparable to the baseline levels (**Figure** 6A). Subsequently, we performed a comprehensive serum chemistry panel, and the results remained consistent with the baseline levels (Figure 6B). These findings from blood analysis showed the short-term safety of PLT-NDs in vivo. Moreover, we collected tissues from the heart, liver, spleen, lung, and kidney and conducted histological analysis after sectioning and staining with hematoxylin and eosin (H&E). The histological analysis revealed similar appearances between the control and treated mice, without any apparent irregularities or signs of acute toxicity caused by PLT-ND (Figure 6C). These results collectively indicated that PLT-NDs had good biosafety.

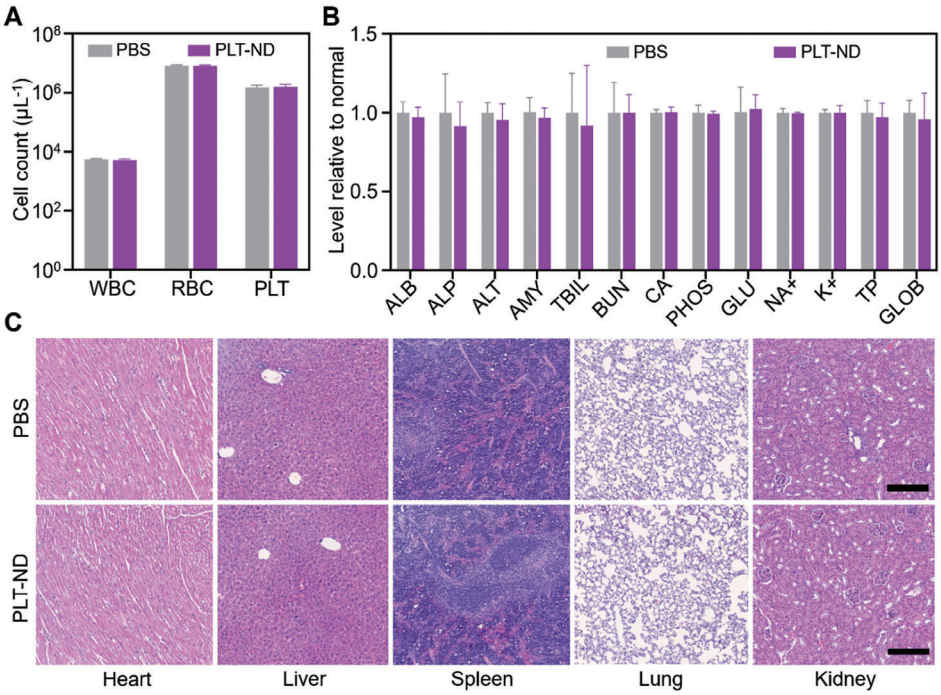

Figure 6. In vivo biosafety of PLT-NDs. A) Counts of various blood cells 24 h after intravenous injection of PBS (control) or PLT-NDs (30 mg kg^{-1}). WBC, white blood cells; RBC, red blood cells. PLT, platelets. B) Blood biochemical panel analysis after 24 h administration of PBS or PLT-NDs. ALB, albumin; ALP, alkaline phosphatase; ALT, alanine transaminase; AMY, amylase; TBIL, total bilirubin; BUN, blood urea nitrogen; CA, calcium; PHOS, phosphorus; GLU, glucose; NA+, sodium; K+, potassium; TP, total protein; GLB, globulin. C) H&E staining of histology sections from major organs (heart, liver, spleen, lung, and kidney) after 24 h administration of PBS or PLT-NDs. Scale bar = 100 μm. Two groups of data were analyzed by using a Student's *t*-test (two-tailed), and the comparison between PBS and PLT-ND groups was not statistically significant ($p > 0.05$). In all studies, $n = 3$ mice, and data are presented as mean + s.d.

3. Conclusion

In summary, we successfully developed an innovative PLT-ND formulation using platelet membranes and demonstrated their broad neutralization capability against various biological agents associated with different diseases. PLT-NDs were significantly smaller than the original platelet membrane vesicles and stable in biological solutions. They were able to effectively bind and neutralize anti-platelet autoantibodies both in vitro and in vivo, displaying strong potential for the treatment of ITP. In an MRSA infection model, PLT-NDs were shown to effectively neutralize both purified toxins and complex wSP in vitro and in vivo, leading to significant survival benefits. Biosafety studies further revealed that PLT-NDs had negligible acute toxicity on molecular, cellular, and tissue levels. Collectively, these results underscore the versatile capabilities of PLT-NDs for bioneutralization, positioning them as a promising therapeutic platform for immune thrombocytopenia and bacterial infections. PLT-NDs represent a unique platelet-mimicking nanomedicine platform, offering a promising prospect for various biomedical applications by harnessing the biological functions of platelet membranes.

4. Experimental Section

Animal Care: All animal studies were approved under the guidelines of the University of California San Diego (UCSD) Institutional Animal Care and Use Committee (IACUC). All animal studies used 6-week-old ICR mice (male and female, Harlan Laboratories, male). Mice were housed in an animal facility at UCSD under federal, state, local, and National Institutes of Health (NIH) guidelines for animal care.

Platelet Collection and Platelet Membrane Derivation: Mouse whole blood was collected from the mice via submandibular vein puncture into microcentrifuge tubes coated with heparin (Fisher Scientific). The blood sample was centrifuged at 300 × g for 5 min at room temperature to separate the blood components into three layers: platelet-poor plasma (PPP) on the top, a buffy coat in the middle, which contains white blood cells (WBCs) and platelets, and red blood cells (RBCs) at the bottom. The buffy coat and the PPP layer were collected as platelet-rich plasma (PRP). Then, PRP was centrifuged at 2000 × *g* for 4 min. After the supernatant was removed, the platelets were resuspended in 1× PBS, aliquoted, and stored in a −80 °C freezer for future use. To derive the platelet membrane, frozen platelets were thawed at room temperature, centrifuged at 8000 × g for 7 min, and the pellet was resuspended in water. The pellet suspension was refrozen and thawed, and the freeze-thaw cycle was repeated thrice. Finally, the suspension was centrifuged at 21 000 × g for 10 min, and the membrane pellet was resuspended in water. The membrane protein concentration was quantified with a bicinchoninic acid (BCA) protein assay kit (Pierce, Thermo Fisher Scientific). The sample was stored at −80 °C for future use.

Synthesis and Characterization of PLT-NDs: The platelet membrane was first sonicated to form platelet membrane vesicles (Fisherbrand Model 120 Sonic Dismembrator, 100 W for 30 s). Then the vesicles were mixed with styrene-maleic acid copolymer-lipid particles 200 (SMALP 200, Cube Biotech) at a membrane protein-to-polymer weight ratio of 1:5. The mixture was sonicated (Fisherbrand Model 120 Sonic Dismembrator, 100 W) in an ice water bath for 30 s. The sample was stirred overnight at 4 °C and centrifuged at 150 000 × g for 30 min. The supernatant

containing PLT-NDs was taken. The PLT-NDs in the supernatant were washed and concentrated with an Amicon filtration tube (10 kDa MWCO).

Synthesis of N_3-PLT-NDs: To synthesize N_3-PLT-NDs, platelet membrane was mixed with 1,2-distearoyl-sn-glycero-3-phosphoethanolamine-N-(azido(polyethylene glycol)−2000) (DSPE-PEG2000-N_3, Nanosoft Biotechnology) at a membrane protein-to-polymer weight ratio (500:1), incubated at 37 °C for 1 h. Then the mixture was centrifuged at 10 000 × *g* for 10 min. Azido (N3)-functionalized platelet membrane was collected as the pellet. The membrane was used to synthesize azido-functionalized PLT-NDs with the same procedure described above. To label the NDs with Alexa Fluor647 (Ex/Em = 650/668), PLT-NDs were incubated with Alexa Fluor647-NHS ester (Thermo Fisher Scientific), followed by purification with an Amicon filtration tube (10 kDa MWCO). To label PLT-ND with 1,1″-dioctadecyl-3,3,3″,3'-tetramethylindocarbocyanine perchlorate (DiL, Ex/Em = 495/519), platelet membrane was mixed with DiL (0.02 wt%) and sonicated before being used to prepare DiL-labeled PLT-NDs (denoted "DiL-PLT-NDs").

PLT-ND Characterization: The size and surface zeta potential were measured with dynamic light scattering (DLS, Malvern ZEN 3600 Zetasizer, at 0.5 mg mL^{-1}). For PLT-ND morphology, samples were negatively stained with 1% uranyl acetate (Electron Microscopy Sciences) and visualized using a JEOL 1200 EX II transmission electron microscope (TEM, JEOL 1200 EX II). For the stability test, PLT-ND samples (1 mL, 1 mg mL^{-1}) were incubated in 50% fetal bovine serum (FBS, Hyclone) at 37 °C. Their sizes were measured with DLS at various time points (0, 12, 24, 36, 48, 60, and 72 h). For extended stability, PLT-ND samples (1 mL, 1 mg mL^{-1}) were incubated in 1× PBS at 4 °C, and their sizes were measured daily for 7 d with DLS. To characterize PLT-ND pharmacokinetic (PK) profile, Alexa Fluor647-labeled PLT-NDs (30 mg kg^{-1} of protein weight) were injected via the tail vein (n = 3), and blood samples were collected at predetermined time points (1, 5, 15, and 30 min, and 1, 4, 8, 24, and 48 h). After the blood collection, fluorescence intensity was measured (Tecan M200). To fit the pharmacokinetic profile with a two-compartment model, the data points corresponding to the elimination phase were first selected. By fitting the points linearly, the slope (k) was determined. Then the elimination constant $\beta = -2.303k$ was obtained. The elimination half-life ($t_{1/2}$) was calculated to be $t_{1/2} = \mathrm{Ln}2/\beta$. To characterize PLT-ND biodistribution, Alexa 647-labeled PLT-ND (30 mg kg^{-1}, protein weight) was injected intravenously through the tail vein. At 24, 48, and 72 h after the injection, major organs, including the liver, kidneys, spleen, brain, lungs, heart, and blood, were collected from the mice (n = 3). The collected organs were then weighed and homogenized in 1× PBS for fluorescence measurement (Tecan M200). The measured intensity was multiplied by the corresponding organ weight to obtain the total organ fluorescence. Then the relative distribution of the PLT-NDs in each organ was calculated.

Synthesis of RBC-NDs: Human RBCs (ZenBio, Inc) were washed with ice-cold 1× PBS and then suspended in hypotonic 0.25× PBS on ice for 20 min for lysis. Lysed cells were centrifuged at 800 × *g* for 5 min, followed by hemoglobin removal. The hypotonic treatment was repeated thrice, and the emptied RBC ghosts were collected as pale pink pellets. The collected membrane was suspended in water, and the protein concentration was quantified with BCA assay following the vendor's protocol. The collected RBC membrane ghost was aliquoted and stored at −80 °C for subsequent studies. RBC-NDs were synthesized using the same procedure as PLT-NDs. Meanwhile, RBC-NDs were labeled with azido group (N_3-RBC-NDs) or DiL (DiL-RBC-NDs) using the same procedures as N_3-PLT-NDs and DiL-PLT-NDs.

Anti-Platelet Antibody (PLT-Ab) Binding Study: To study the binding specificity, N_3-PLT-NDs or N_3-RBC-NDs (both at 10 μg mL^{-1}) were mixed with fluorescein isothiocyanate (FITC)-labeled polyclonal anti-mouse thrombocyte antibodies (FITC-PLT-Abs, 30 μg mL^{-1}) for 10 min at 37 °C either in 1× PBS or 50% mouse serum. Then, the mixture was added with agarose beads functionalized with dibenzocyclooctyl (DBCO, bead final concentration = 40 μg mL^{-1}), which served as a tool to separate NDs from the suspension. The sample was incubated for 30 min at room temperature. The mixture was centrifuged at 20000 × g for 1 min to spin down the beads. The pellet was resuspended in 1× PBS, and the fluorescence intensity was measured (Tecan M200). The intensity measured from PLT-NDs was defined as 100%. To study the binding capacity, the antibody (30 μg mL^{-1}) was mixed with N_3-PLT-NDs (0–8 μg mL^{-1}, twofold dilutions) for 10 min at 37 °C in 1× PBS. Then, the mixture was added with agarose beads (40 μg mL^{-1}) for 30 min at room temperature. After the incubation, the mixture was centrifuged at 20000 × g for 1 min to spin down the beads while pulling down the PLT-ND/antibody complexes. To measure the PLT-ND-antibody dissociation affinity, the PLT-ND (25 μg mL^{-1}) was mixed with twofold dilutions of antibody (1.56–400 μg mL^{-1}) for 10 min at 37 °C in 1× PBS. Then, the mixture was added with agarose beads (40 μg mL^{-1}) for 30 min at room temperature. After the incubation, the mixture was centrifuged at 20 000 × g for 1 min to spin down the beads while pulling down the PLT-ND/antibody complexes. The pellet was resuspended in 1× PBS, and the fluorescence intensity was measured (Ex/Em = 495/519, Tecan M200). Based on the fluorescence intensity, the amount of antibody bound to the PLT-NDs was calculated.

In Vitro Inhibition of PLT-Ab Binding with Platelets: To study the inhibition, 1× PBS or PLT-NDs (10 μg mL^{-1}) was added to FITC-PLT-Abs (final concentration 20 μg mL^{-1}) at 37 °C for 15 min. The mixture was then added to a platelet suspension (≈4 × 10^6 platelet mL^{-1}, equivalent to 40 μg of membrane material). The mixture was incubated at 37 °C for 15 min and then washed with 1× PBS thrice by centrifugation at 2000 × g and imaged by LSCM (Leica SP8). The platelet only served as a control group. To measure the inhibition quantitatively, two regimens were adopted. In a pre-incubation regimen, twofold dilutions of PLT-NDs (0–16 μg mL^{-1}) were added to FITC-PLT-Abs (final concentration 20 μg mL^{-1}) at 37 °C for 15 min. The mixture was then added to a platelet suspension (≈4 × 10^6 platelet mL^{-1}, equivalent to 40 μg of membrane material). The mixture was incubated at 37 °C for 15 min and then washed with 1× PBS thrice by centrifugation at 2000 × g. The antibody bound to platelets was measured by flow cytometry on a Becton Dickinson FACSCanto II flow cytometer and analyzed using Treestar Flowjo. In a competitive regimen, twofold dilutions of PLT-ND (0–32 μg mL^{-1}) and FITC-Ab were simultaneously added to the platelet suspension (≈4 × 10^6 platelet mL^{-1}). The antibody bound to platelets was measured with the same procedure as that in the pre-incubation regimen.

In Vivo Neutralization of PLT-Abs by PTL-NDs: A mouse model of thrombocytopenia was established by injecting PLT-Abs (50 μg) into the mice intraperitoneally.[29] To evaluate PLT-ND effectiveness, 50 μg of PLT-Abs were injected into the mice intraperitoneally. After 15 min, mice were injected with various dosages of PLT-NDs (0, 5, 10, and 20 mg kg^{-1}) via the tail vein. Mice intravenously injected with 1× PBS were used as a sham control. Blood samples were collected before and 24 h after antibody administration, and the platelet was counted. For platelet enumeration, 1 μL blood was diluted 1000 times in 1× PBS containing 1%v/v bovine serum albumin (BSA, Millipore-Sigma). The diluted solution was then added with FITC-labeled anti-mouse CD41 (Biolegend) to label the platelets. Flow cytometry was used to count the number of FITC+ events per given volume. To evaluate PLT-ND effectiveness based on bleeding time, mice were anesthetized 24 h after the antibody administration with a combination of ketamine (80 mg kg^{-1}, Zoetis) and xylazine (10 mg kg^{-1}, Lloyd Laboratories). To measure the bleeding time, a tail segment 5 mm from the distal end was excised with a sterile blade. The cut end was placed into a 37 °C saline solution immediately. The time from amputation to complete bleeding cessation was recorded for each mouse. Mice bleeding longer than 20 min were euthanized. For PLT recovery kinetics, mice were injected intraperitoneally with PLT-Abs (50 μg per mouse). After 15 min, mice were injected with PLT-NDs (10 mg kg^{-1}) via the tail vein. Mice intravenously injected with 1× PBS or PLT-Abs (50 μg) were used as the controls. Blood samples were collected before antibody administration and at 3, 6, 12, and 24 h after antibody administration.

Preparation of MRSA Whole Secreted Proteins (wSP): MRSA USA300 stock (ATCC) was inoculated onto a tryptic soy broth (TSB) agar plate and incubated at 37 °C for 24 h. Then a single colony was transferred from the agar plate into 4 mL TSB, followed by incubation at 37 °C with gentle shaking for 12 h. Then, the bacterial culture was transferred to 10 mL fresh TSB and incubated at 37 °C until the concentration reached ≈1 × 10^9 CFU mL^{-1} (OD600 = 1 corresponds to 1 × 10^8 CFU mL^{-1} bacteria). The bacterial culture was centrifuged at 5000 × g for 10 min. The supernatant was

passed through a 0.22 µm membrane filter. The MRSA supernatant containing wSP was stored at −80 °C for future experiments.

In Vitro Platelet Cytotoxicity and Activation Assays: For the cytotoxicity study, mouse platelets (1×10^7 in 20 µL 1× PBS per well) were seeded in a 96-well plate in 170 µL of serum-free RPMI 1640 media (Thermo Fisher Scientific) at room temperature. PLT-ND (8 µL, 40 µg mL^{-1} final concentration) was mixed with α-toxin (2 µL, 4 µg mL^{-1} final concentration) or MRSA wSP (2 µL), and the mixture was incubated at 37 °C for 10 min. Then, the mixture was added to each well and incubated at 37 °C for 30 min. After the incubation, platelet samples were centrifuged at 500 × g for 5 min, and 150 µL of the supernatant was taken for the lactate dehydrogenase (LDH) assay (Millipore-Sigma). Platelets added with 1× PBS served as a negative control, while platelets added with α-toxin or MRSA wSP were positive controls. For the platelet activation study, PLT-ND (8 µL, 40 µg mL^{-1} final concentration) was mixed with MRSA wSP (2 µL) at 37 °C for 10 min. Then, the mixture was added to each well and incubated at 37 °C for 15, 30, and 60 min. Platelets added with 1× PBS or MRSA wSP served as controls. After the incubation, the samples were stained with phycoerythrin (PE) anti-mouse P-selectin antibody (Biolegend) for the detection of P-selectin with flow cytometry (Becton Dickinson FACSCanto II flow cytometer). Data was analyzed with Treestar Flowjo.

In Vitro Macrophage Cytotoxicity Assay: J774 cells, a murine macrophage cell line (ATCC), were seeded in a 96-well plate in Dulbecco's Modified Eagle Medium (DMEM, Thermo Fisher Scientific) containing 1% penicillin-streptomycin and 10% FBS at 1×10^5 cells per well and allowed to adhere overnight. Then, the medium in the well was removed and replaced with 190 µL of fresh culture medium. PLT-ND (8 µL, 40 µg mL^{-1} final concentration) was mixed with α-toxin (2 µL, 4 µg mL^{-1} final concentration) or MRSA wSP (2 µL) at 37 °C for 10 min, respectively. Then, the mixture was added into the 96-well and incubated at 37 °C for 30 min. After the incubation, 150 µL of culture medium was taken for the LDH assay (Millipore-Sigma). Cells added with 1× PBS, α-toxin, or MRSA wSP were the controls.

In Vitro Macrophage Oxidative Burst and Nitric Oxide Production Assays: J774 cells were seeded in a 96-well plate (1×10^5 cells/well) in DMEM containing 1% penicillin-streptomycin and 10% FBS. The cells were cultured at 37 °C for 12 h. For oxidative burst assays, J774 cells were incubated with 25 µM 2,7-dichlorofluorescein diacetate (DCFH-DA, Thermo Fisher Scientific) in Hank's balanced salt solution (HBSS, Mediatech) lacking Ca^{2+} and Mg^{2+} at room temperature for 30 min. Then, the medium in the wells was removed and replaced with 180 µL of fresh culture medium. PLT-ND (10 µL, 40 µg mL^{-1} final concentration) was mixed with MRSA (10 µL in 1× PBS, 1×10^6 CFU/well) at 37 °C for 10 min. Then, the mixture was added into each well and incubated at 37 °C for 15, 30, 45, 60, 90, and 120 min. The fluorescence intensity was measured at different times (Ex/Em = 485/520, Tecan M200). For the nitric oxide production assay, the medium in the wells was removed and replaced with 180 µL of fresh culture medium. PLT-ND (10 µL, 40 µg mL^{-1} final concentration) was mixed with 1×10^6 CFU MRSA (10 µL in 1× PBS) at 37°C for 10 min. Then, the mixture was added into each well and incubated at 37 °C for 2, 4, 8, and 12 h. After the incubation, 100 µL of supernatant was removed, and 100 µL of Greiss reagent (Promega) was added. The absorbance of nitrite-containing samples was measured at 550 nm (Tecan M200). For the standard curve, sodium nitrite standard (100 µL in 1× PBS, 100 µM final concentration) was twofold diluted, and 100 µL of Greiss reagent was added to each dilution. The absorbance of nitrite standards was measured at 550 nm. A standard curve was generated by plotting the concentration against the absorbance. The nitrite concentrations in samples were calculated using the standard curve. In both assays, J774 cells added with 1× PBS or MRSA only served as the negative and positive control, respectively.

In Vitro Macrophage Bactericidal Assays: J774 cells were seeded in 96-well plates at 1×10^5 cells/well and allowed to adhere overnight. Then, the medium in the wells was removed and replaced with 180 µL of fresh culture medium. PLT-ND (10 µL, 40 µg mL^{-1} final concentration) or 1× PBS (10 µL) was mixed with 1×10^6 CFU MRSA (10 µL in 1× PBS) at 37 °C for 10 min. Then, the mixture was added to each well and incubated at 37 °C for 2 h. Following the incubation, the cells were gently washed with warm 1× PBS, and then a medium containing 100 µg mL^{-1} gentamicin (Millipore-Sigma) was added. The samples were incubated for 3 h to eliminate extracellular bacteria. The viable intracellular bacteria were quantified by first disrupting J774 cells using a hypotonic solution of 10 mM Tris-HCl (pH 7.4) and 1 mM ethylenediaminetetraacetic acid (EDTA). Then a series of tenfold dilutions from the disrupted cell suspension was inoculated to TSB agar plates. The agar plates were cultured at 37 °C for 24 h, and the colony formation was counted.

In Vivo Inhibition of MRSA Infection by PLT-ND: For MRSA lethal dosage determination, MRSA USA300 of various dosages (1×10^8–3×10^8 CFU) was injected intraperitoneally into the mice. A lethal dosage of 100% (LD100) and a median lethal dose (LD50) were determined by observing mouse survival for 120 h. For PLT-ND effectiveness measurement, 2×10^8 CFU of MRSA USA300 was first injected intraperitoneally into the mice. PLT-NDs (10, 20, and 30 mg kg^{-1}) were intravenously injected through the tail vein 1 min after the MRSA injection. Furthermore, PLT-ND effectiveness was also examined by injecting the mice with MRSA intraperitoneally (3×10^8 CFU/mouse), followed by injecting PLT-NDs intravenously (10, 20, and 30 mg kg^{-1}) twice at 1 min and 24 h after MRSA injection, respectively. Mouse survival was monitored for 120 h.

In Vivo Acute Toxicity Study: PLT-NDs (10 mg mL^{-1}, protein concentration) were injected intravenously through the tail vein into the mice at 30 mg kg^{-1}. After 24 h, ≈350 µL of the blood was collected via submandibular puncture. The first 250 µL blood was placed into Eppendorf tubes and allowed to coagulate. The following 100 µL blood was collected into an ethylenediaminetetraacetic acid (EDTA, Hyclone)-coated microtube. The first sample containing 250 µL blood was centrifuged at 2500 × g for 3 min to collect the serum for comprehensive metabolic panel analysis. The second sample containing 100 µL blood was used for the complete blood count without processing. All blood samples were analyzed at the UCSD Animal Care Program Diagnostic Services Laboratory. Meanwhile, immediately after the blood collection, mice were euthanized. The major organs were collected, including the heart, liver, spleen, lung, and kidney. Organs were fixed with 10% formalin, sectioned, and stained with hematoxylin and eosin for histological analysis. Histology slides were imaged with a Micromaster II microscope (Fisher Scientific). Mice that received PBS served as controls.

Acknowledgements

This work was supported by the Defense Threat Reduction Agency Joint Science and Technology Office for Chemical and Biological Defense under award number HDTRA1-21-1-0010.

Conflict of Interest

The authors declare no conflict of interest.

Data Availability Statement

The data that support the findings of this study are available from the corresponding author upon reasonable request.

Keywords

biological neutralization, cell membrane, cellular nanodisc, nanomedicine, platelet

Received: September 20, 2023
Revised: November 8, 2023
Published online: December 3, 2023

[1] B. Ho-Tin-Noé, Y. Boulaftali, E. Camerer, *Blood* **2018**, *131*, 277.
[2] J. W. Semple, J. E. Italiano, J. Freedman, *Nat. Rev. Immunol.* **2011**, *11*, 264.
[3] H. Hamzeh-Cognasse, P. Damien, A. Chabert, B. Pozzetto, F. Cognasse, O. Garraud, *Front. Immunol.* **2015**, *6*, 82.
[4] Q. Hu, H. N. Bomba, Z. Gu, *Front. Chem. Sci. Eng.* **2017**, *11*, 624.
[5] F. Yang, Z. Kong, Q. Ji, S. Li, J. Sun, Z. He, S. Zhang, C. Luo, *ACS Mater. Lett.* **2023**, *5*, 429.
[6] Q. Hu, W. Sun, C. Qian, C. Wang, H. N. Bomba, Z. Gu, *Adv. Mater.* **2015**, *27*, 7043.
[7] A. C. Anselmo, C. L. Modery-Pawlowski, S. Menegatti, S. Kumar, D. R. Vogus, L. L. Tian, M. Chen, T. M. Squires, A. Sen Gupta, S. Mitragotri, *ACS Nano* **2014**, *8*, 11243.
[8] X. Liu, F. Zhang, Q. Wang, J. Gao, J. Meng, S. Wang, Z. Yang, L. Jiang, *Small* **2014**, *10*, 4677.
[9] C.-M. J. Hu, R. H. Fang, K.-C. Wang, B. T. Luk, S. Thamphiwatana, D. Dehaini, P. Nguyen, P. Angsantikul, C. H. Wen, A. V. Kroll, C. Carpenter, M. Ramesh, V. Qu, S. H. Patel, J. Zhu, W. Shi, F. M. Hofman, T. C. Chen, W. Gao, K. Zhang, S. Chien, L. Zhang, *Nature* **2015**, *526*, 118.
[10] S. Wang, Y. Duan, Q. Zhang, A. Komarla, H. Gong, W. Gao, L. Zhang, *Small Struct* **2020**, *1*, 2000018.
[11] J. Zhuang, H. Gong, J. Zhou, Q. Zhang, W. Gao, R. H. Fang, L. Zhang, *Sci. Adv.* **2020**, *6*, eaaz6108.
[12] Y. Zhou, Q. J. Liang, X. J. Wu, S. Z. Duan, C. L. Ge, H. Ye, J. H. Lu, R. Y. Zhu, Y. B. Chen, F. H. Meng, L. C. Yin, *Adv. Mater.* **2023**, *35*, 10691.
[13] J. Xu, Y. Zhang, J. Xu, G. Liu, C. Di, X. Zhao, X. Li, Y. Li, N. Pang, C. Yang, Y. Li, B. Li, Z. Lu, M. Wang, K. Dai, R. Yan, S. Li, G. Nie, *Adv. Mater.* **2020**, *32*, 1905145.
[14] U. D. S. Sekhon, K. Swingle, A. Girish, N. Luc, M. De La Fuente, J. Alvikas, S. Haldeman, A. Hassoune, K. Shah, Y. Kim, S. Eppell, J. Capadona, A. Shoffstall, M. D. Neal, W. Li, M. Nieman, A. Sen Gupta, *Sci. Transl. Med.* **2022**, *14*, eabb8975.
[15] S. Roullet, N. Luc, J. Rayes, J. Solarz, D. Disharoon, A. Ditto, E. Gahagan, C. Pawlowski, T. Sefiane, F. Adam, C. Casari, O. D. Christophe, M. Bruckman, P. J. Lenting, A. Sen Gupta, C. V. Denis, *Blood* **2023**, *141*, 2891.
[16] A. Girish, K. Jolly, N. Alsaadi, M. De La Fuente, A. Recchione, R. An, D. Disharoon, Z. Secunda, S. Raghunathan, N. F. Luc, C. Desai, E. Knauss, X. Han, K. Hu, H. Wang, U. D. S. Sekhon, N. Rohner, U. A. Gurkan, M. Nieman, M. D. Neal, A. Sen Gupta, *ACS Nano* **2022**, *16*, 16292.
[17] I. Noh, Z. Guo, J. Zhou, W. Gao, R. H. Fang, L. Zhang, *ACS Nano* **2023**, *17*, 1120.
[18] L. Sun, D. Wang, I. Noh, R. H. Fang, W. W. Gao, L. F. Zhang, *Angew. Chem., Int. Ed.* **2023**, *62*, e2023015.
[19] T. H. Bayburt, S. G. Sligar, *FEBS Lett.* **2010**, *584*, 1721.
[20] I. G. Denisov, S. G. Sligar, *Nat. Struct. Mol. Biol.* **2016**, *23*, 481.
[21] R. Kuai, L. J. Ochyl, K. S. Bahjat, A. Schwendeman, J. J. Moon, *Nat. Mater.* **2017**, *16*, 489.
[22] N. Doshi, J. N. Orje, B. Molins, J. W. Smith, S. Mitragotri, Z. M. Ruggeri, *Adv. Mater.* **2012**, *24*, 3864.
[23] S. Sun, R. T. Urbanus, H. Ten Cate, P. G. De Groot, B. De Laat, J. W. M. Heemskerk, M. Roest, *Cells* **2021**, *10*, 3386.
[24] M. Swinkels, M. Rijkers, J. Voorberg, G. Vidarsson, F. W. G. Leebeek, A. J. G. Jansen, *Front. Immunol.* **2018**, *9*, 880.
[25] B. A. Diep, M. Otto, *Trends Microbiol.* **2008**, *16*, 361.
[26] N. Ahmad-Mansour, P. Loubet, C. Pouget, C. Dunyach-Remy, A. Sotto, J.-P. Lavigne, V. Molle, *Toxins* **2021**, *13*, 677.
[27] O. Vilanova, J. J. Mittag, P. M. Kelly, S. Milani, K. A. Dawson, J. O. Rädler, G. Franzese, *ACS Nano* **2016**, *10*, 10842.
[28] F. Alves-Rosa, C. Stanganelli, J. Cabrera, N. Van Rooijen, M. S. Palermo, M. N. A. Isturiz, *Blood* **2000**, *96*, 2834.
[29] X. Wei, J. Gao, R. H. Fang, B. T. Luk, A. V. Kroll, D. Dehaini, J. Zhou, H. W. Kim, W. Gao, W. Lu, L. Zhang, *Biomaterials* **2016**, *111*, 116.
[30] M. Morowski, T. Vögtle, P. Kraft, C. Kleinschnitz, G. Stoll, B. Nieswandt, *Blood* **2013**, *121*, 4938.
[31] M. Otto, *Cell. Microbiol.* **2012**, *14*, 1513.
[32] A. V. Fejes, M. G. Best, W. A. Van Der Heijden, A. Vancura, H. Verschueren, Q. De Mast, T. Wurdinger, C. Mannhalter, *Sci. Rep.* **2018**, *8*, 16145.
[33] J. K. Kim, S. Uchiyama, H. Gong, A. Stream, L. F. Zhang, V. Nizet, *Engineering* **2021**, *7*, 1149.
[34] J. Fu, Y. Li, Y. Zhang, Y. Liang, Y. Zheng, Z. Li, S. Zhu, C. Li, Z. Cui, S. Wu, *Adv. Mater.* **2021**, *33*, 2102926.
[35] M. Herb, M. Schramm, *Antioxidants* **2021**, *10*, 313.
[36] E. M. Palmieri, C. Mcginity, D. A. Wink, D. W. Mcvicar, *Metabolites* **2020**, *10*, 429.